THE JOURNAL OF PHYSICAL CHEMISTRY B

Article

pubs.acs.org/JPCB

Microstructures and Interaction Analyses of Phosphonium-Based Ionic Liquids: A Simulation Study

Xiaomin Liu,[†] Yuling Zhao,[†,‡] Xiaochun Zhang,[†] Guohui Zhou,[§] and Suojiang Zhang*[,†]

[†]State Key Laboratory of Multiphase Complex Systems, Institute of Process Engineering, Chinese Academy of Sciences, Beijing, 100190, China

[‡]Key Laboratory of Green Chemical Media and Reactions, Ministry of Education, School of Chemistry and Environmental Science, Henan Normal University, Xinxiang, Henan 453007, China

[§]Beijing Salien Company, Beijing, 100083, China

Supporting Information

ABSTRACT: Simulation study of eight kinds of phosphonium-based ionic liquids (ILs) is reported in this work. Force fields for two kinds of alkoxyphosphonium ILs are proposed through systematic method and validated by the experimental densities. The study was conducted by molecular dynamics simulations. A connection between the intermolecular energy, divided into the electrostic force and the van der Waals force, and the experimental viscosities was found. Radial distribution functions (RDFs) were analyzed to probe the local organization of the liquids. First-shell coordination numbers are also reported by integral of RDFs from zero to the first minimum. In order to compare the interaction strength and position between ions for different kinds of ILs, the relative density distributions along with the distance between cation and anion are proposed. Hydrogen bond numbers were investigated to depict the microinteraction. We found that, although there are six anions in the first solvation shell of $[P_{2,2,2,5}]^+$, only one hydrogen bond could be found. Along with increase in the length of alkyl chain, the hydrogen bond number becomes less, and no hydrogen bond interaction is found for 20% of the ions in $[P_{4,4,4,14}][Tf_2N]$ In order to depict the effect of carbon chain length on the structure, the space distribution functions were also computed and compared.

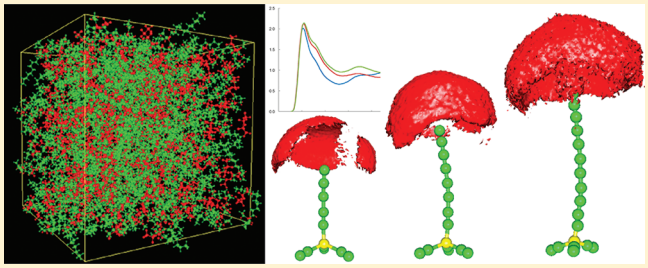

1. INTRODUCTION

Phosphonium-based ionic liquids (ILs), many of which are composed of the relatively large number and volume-occupying alkyl side chains, are well-known for their chemical and thermal stabilities which are practical advantages for various applications. For example, they have been reported useful in several electrochemical applications, such as voltammetric measurements for various redox couples,[1] anodic polymerization of pyrrole,[2] supercapacitors,[3] and dye-sensitized solar cells.[4,5] Recently, the phosphonium-based ILs containing a methoxy group, triethyl(methoxymethyl)phosphonium bis(trifluoromethylsulfonyl)imide and triethyl(2-methoxyethyl)-phosphonium bis(trifluoromethylsulfonyl)imide, were proved to exhibit quite low viscosities and could be used as the novel electrolyte.[6] In order to make good use of these phosphonium-based ILs and also design task-specific ILs with great versatility of chemical and physical properties, it is urgent for us to explore their relationship between microstructures and macroproperties. For example, Walden plot was applied to several phosphonium-based ILs, and it indicated that some ILs may appear to be of relatively low degree of ionicity due to the strong ion pairing.[7] This innovational finding will lead to further enlarging of the range of physical-chemical properties and tuning by modifications of the ILs' chemical architecture.[8]

Molecular simulations have been proved indispensable for the understanding of phosphonium-based ILs at the molecular level.[9] For example, $[P_{6,6,6,14}]Cl$ was studied by Gontrani et al. using molecular dynamics simulations and small- and wide-angle X-ray scattering and strong P−Cl interaction and nanoscale segregation.[8] Velocity autocorrelation function and mean-square displacement were applied to study dynamics properties for ILs composed of $[P_{4,4,4,4}]^+$ with amino acid anions, and chemical functionality and the alkyl chain length of the anion were found to be the major factors for determining the transport coefficients.[10] Zhou et al. have performed molecular simulations on 14 kinds of tetrabutylphosphonium ILs coupling $[P_{4,4,4,4}]^+$ with amino acid anions, and radial distribution functions (RDFs) were investigated to depict the microscopic structures.[11]

Although molecular simulations have been proved useful to understand the behavior of the molecules and the properties of the system, the quality of simulations depends on the force field, which refers to the functional form and parameters set used to describe the potential energy of a system. There are

Received: November 7, 2011
Revised: March 11, 2012
Published: April 4, 2012

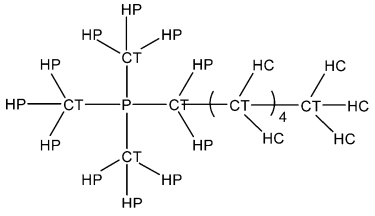

(a) $P_{1,1.1.6}$

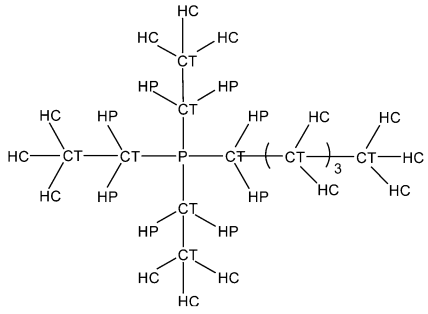

(b) $P_{2,2,2,5}$

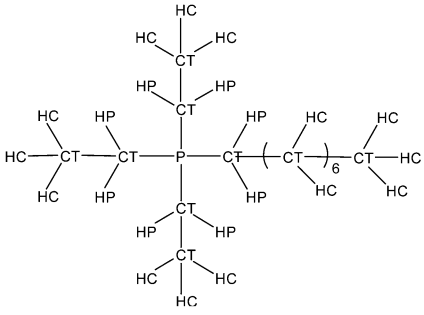

(c) $P_{2,2,2,8}$

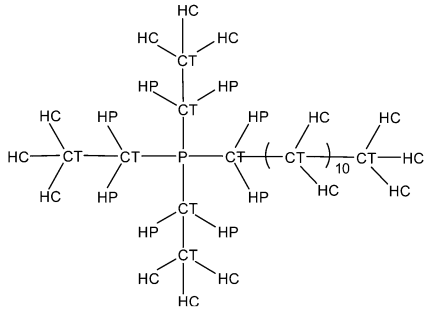

(d) $P_{2,2,2,12}$

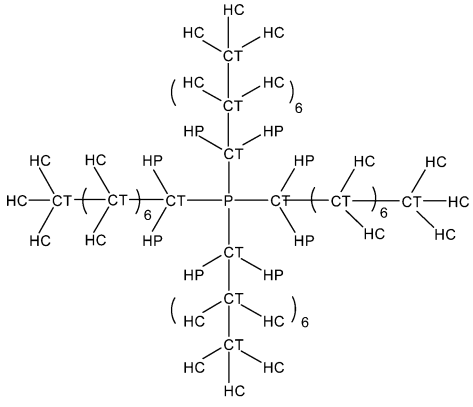

(e) $P_{8,8,8,8}$

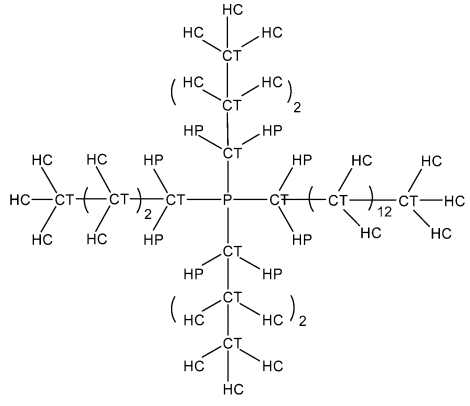

(f) $P_{4,4,4,14}$

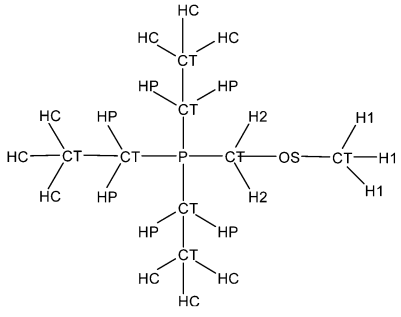

(g) $P_{2,2,2,1O1}$

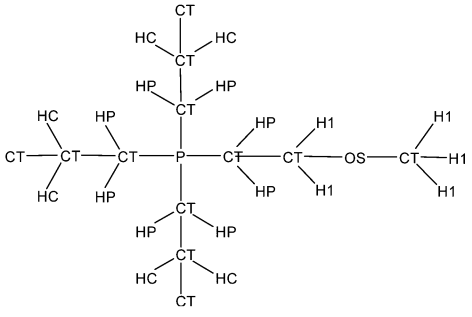

(h) $P_{2,2,2,2O1}$

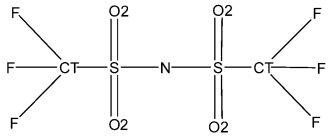

(1) Tf_2N

Figure 1. Atom types for cations and anion.

dx.doi.org/10.1021/jp210696r | J. Phys. Chem. B 2012, 116, 4934−4942

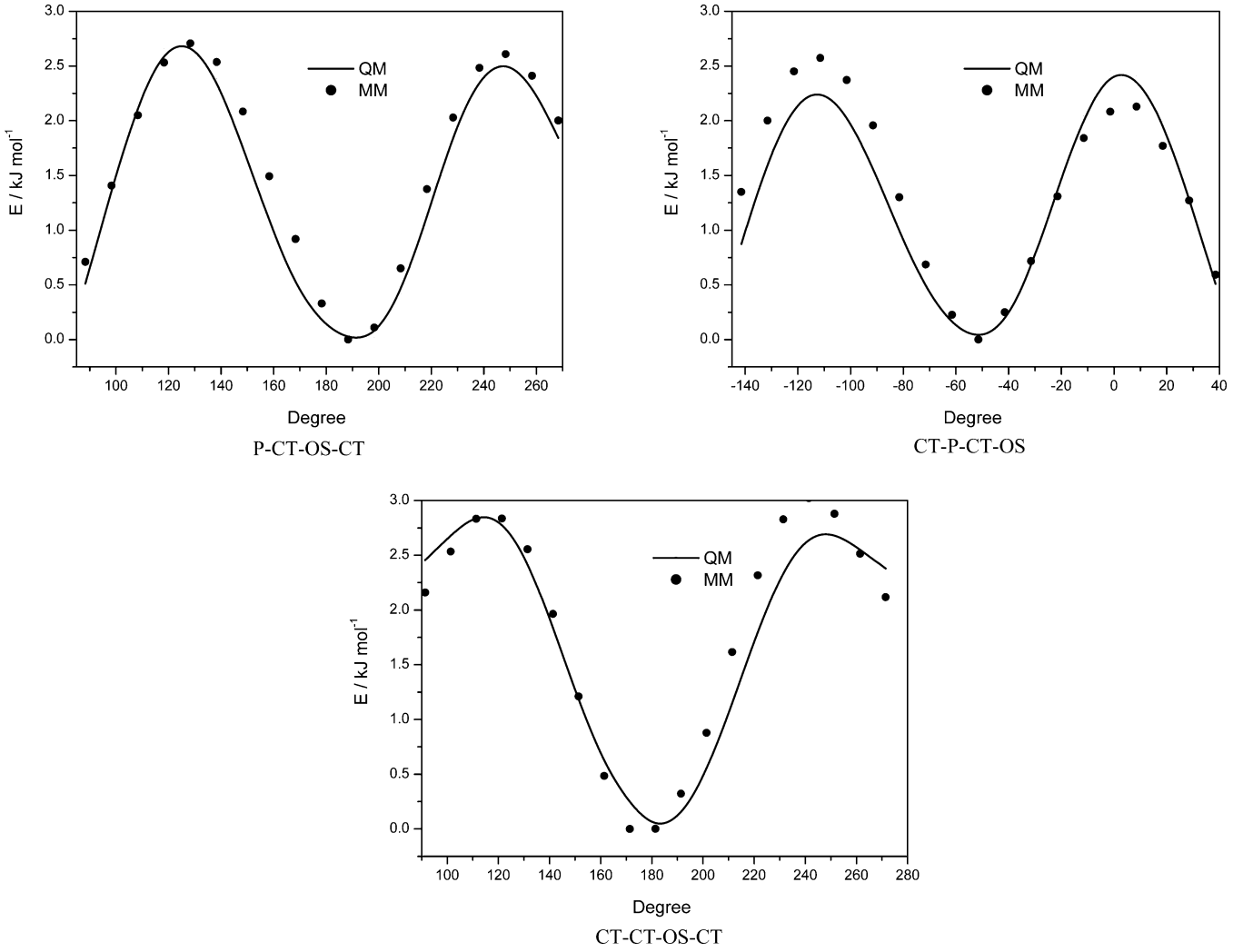

Figure 2. Energy barrier fittings of P-CT-OS-CT, CT-P-CT-OS for $[P_{2,2,2,1O1}]^+$ and CT-CT-OS-CT for $[P_{2,2,2,2O1}]^+$.

three kinds of force fields. "All-atom" (AA) force field provides parameters for every atom in a system, including hydrogen, while "united-atom" (UA) force field treats several atoms as a single interaction center, the most typical example being the hydrogen and carbon atoms in methyl or methylene groups. "Coarse-grained" force field, which is frequently used in long-time simulations of proteins, provides even more abstract representation for increased computational efficiency. Recently, many force fields for ILs have been published.[11−36] Lopes and Padua set up a series of force fields for imidazolium, pyridinium, and phosphonium cations by using the systemic method.[20] Besides, they also proposed the force fields for specific anions, including the triflate, bistriflylimide,[16] chloride, bromide, dicyanamide,[20] alkanesulfonate, alkyl sulfate[31] and also anions with many fluorine atoms, such as bis(fluorosulfonyl)amide, perfluoroalkanesulfonylamide, and fluoroalkylfluorophosphate.[35] Based on the Amber force field, Liu et al also developed a series of force fields for imidazolium-based ILs, and the van der Waals parameters (VDW) were adjusted to refine the force field.[17,36] In order to improve the predicted properties, for example, the dynamic properties, many force fields with polarization term were proposed. Yan et al.[18] used the polarization force field for $[Emim][NO_3]$, and the simulated viscosity is more accurate compared with non-polarization one. Wu et al. and our group have proposed several force fields for guanidinium-based ILs.[24,29,30,37]For phosphonium-based ILs, Lopes and Pádua proposed the tetraalkylphosphonium force field based on the OPLS-AA model.[20] Zhou et al.[11] set up the all-atom force field for $[P_{4,4,4,4}]^+$ based on the Amber model, and a many-body polarizable force field was developed by Oleg Borodin.[34]

In this work, we propose the Amber force field parameters through the systemic method for two kinds of alkoxyphosphonium ILs named triethyl(methoxymethyl)phosphonium bis(trifluoromethylsulfonyl)imide ($[P_{2,2,2,1O1}][Tf_2N]$) and triethyl(2-methoxyethyl)phosphonium bis(trifluoromethylsulfonyl)imide ($[P_{2,2,2,2O1}][Tf_2N]$). Parameters for the other six tetraalkylphosphonium cations, inlcuding $[P_{1,1,1,6}]^+$, $[P_{2,2,2,5}]^+$, $[P_{2,2,2,8}]^+$, $[P_{2,2,2,12}]^+$, $[P_{4,4,4,14}]^+$, $[P_{8,8,8,8}]^+$ were set to be consistent with our previous tetrabutylphosphonium force field.[11] Molecular dynamics simulations were performed at the ambient temperature. The interenergy divided into electrostatic force and van der Waals force was related to the experimental viscosity and a connection was found. Site to site radial distribution functions (RDFs) and first-shell coordination numbers were applied to depict the microscopic structures of these ILs. Relative density distribution along with the distance between cation and anion was used to compare the interaction strength and position between ions for different kinds of ILs. Hydrogen bond numbers were computed and highlighted;

dx.doi.org/10.1021/jp210696r | J. Phys. Chem. B 2012, 116, 4934−4942

although several anions distributed in the first salvation shell of cation, no more than one hydrogen bond could be found in the shell. For the cation with long alkyl chain, maybe no hydrogen bond exists between the ionic pair. The space distribution functions were also computed and compared to depict the effect of carbon chain length on the structure.

2. FORCE FIELDS

A standard molecular mechanics force field with the functional form was used

$$U = \sum_{\text{bonds}} K_r(r - r_0)^2 + \sum_{\text{angles}} K_\theta(\theta - \theta_0)^2 + \sum_{\text{torsions}} \frac{K_\phi}{2}(1 + \cos(n\phi - \gamma)) + \sum_{i=1}^{N}\sum_{j=i+1}^{N}\left\{4\varepsilon_{ij}\left[\left(\frac{\sigma_{ij}}{\gamma_{ij}}\right)^{12} - \left(\frac{\sigma_{ij}}{\gamma_{ij}}\right)^{6}\right] + \frac{q_i q_j}{\gamma_{ij}}\right\} \quad (1)$$

where U represents the total energy of the system. The bond lengths and angles are represented by harmonic potentials with the equilibrium values of r_0 and θ_0. The dihedral angles are represented by traditional cosine series. The Lennard-Jones (LJ) parameters σ_{ij} and γ_{ij} for different atoms are obtained by the Lorentz–Berthelot combining rules.[38] The nonbonded interactions separated by exactly three bonds (1–4 interactions) are reduced by a scale factor, which is optimized as 1/2 for VDW and 1/1.2 for electrostatic interactions.[39]

Force field parameters for $[Tf_2N]^-$ are derived from the literature.[16] Assignments of the atom types for cations are based on the AMBER force field and our previous work.[11,40] Force field parameters are all shown in Figure 1. The VDW parameters are taken from AMBER99.[40] The isolated ionic structures were optimized using the Gaussian 09 package at the B3LYP/6-31+G(d) level. As the restraint electrostatic potential (RESP) charges have been proved to be very efficient and successful for a variety of systems,[40−44] the one-conformation two-step RESP method was used to derive the atom charges by fitting the electrostatic potential generated from QM calculations at B3LYP/6-31+G(d) level. The optimized geometries were used to set equilibrium bond lengths (r_0) and angles (θ_0). Force constants for $[P_{1,1,1,6}]^+$, $[P_{2,2,2,5}]^+$, $[P_{2,2,2,8}]^+$, $[P_{2,2,2,12}]^+$, $[P_{4,4,4,14}]^+$, and $[P_{8,8,8,8}]^+$ are derived from our previous work on $[P_{4,4,4,4}]^+$.[11] The bond and angle force constants for $[P_{2,2,2,1O1}]^+$ and $[P_{2,2,2,2O1}]^+$ were adjusted by fitting vibration frequencies obtained from molecular mechanics (MM), obtained by Tinker calculation,[17,45] to the QM frequencies.[13] The torsion force constants were obtained by fitting the torsion energy profiles based on MM calculation to the QM ones. The ab initio torsion energy profiles were obtained at the MP2/6-31+G(d)// B3LYP/6-31+G(d) level. In the geometry optimization, the appropriate torsions for each of the torsional angles varied in a step of 10° grid while minimizing the energy with respect to all the other degrees of freedom. The optimized conformers from QM calculation were used directly for MM energy profile calculation by Tinker package. In order to make the parameters consistent for all the cations, the common parameters remain the same. The energy barrier fittings of P-CT-OS-CT, CT-P-CT-OS for $[P_{2,2,2,1O1}]^+$ and CT-CT-OS-CT for $[P_{2,2,2,2O1}]^+$ are displayed in Figure 2.

3. SIMULATION DETAILS

Molecular dynamics simulations were performed for eight kinds of ILs contained 256 ion pairs using the M.DynaMix package.[46] The standard periodical boundary conditions with 2/0.5 fs multiple time-step algorithm were applied. Intramolecular forces and long-range forces including LJ and Coulombic interactions were cut off at 15 and 20 Å, respectively. Ewald summation was implemented for Coulombic interactions. The Nose–Hoover[47] NpT ensemble was adopted with coupling constants of 700 and 100 fs. The equilibrium simulations were performed at the ambient temperature (298 K). The equilibrated time lasted for more than 1.0 ns, and each production phase lasted for 4.0 ns. Trajectories were dumped for further analysis. The system sizes changed from 12 000 atoms ($P_{1,1,1,6}Tf_2N$) to nearly 30 000 atoms ($P_{8,8,8,8}Tf_2N$), and the simulation box sizes are listed in table 1.

Table 1. Simulated and Experimental Densities, Box Lengths, and Relative Atomic Densities (RADs)

cation	ρ_{Sim} (g/cm^3)	ρ_{Sim}[a] (g/cm^3)	ρ_{Exp} (g/cm^3)	error	Box-L (Å)	RAD
$[P_{1,1,1,6}]^+$	1.43		1.34	0.067	51.07	1.00
$[P_{2,2,2,5}]^+$	1.35		1.32	0.023	53.18	0.89
$[P_{2,2,2,8}]^+$	1.28		1.26	0.016	55.64	0.77
$[P_{2,2,2,12}]^+$	1.21		1.21	0.000	59.30	0.64
$[P_{4,4,4,14}]^+$	1.12	1.125	1.112[a]	0.012	64.65	0.49
$[P_{8,8,8,8}]^+$	1.07	1.076	1.071[a]	0.005	68.11	0.42
$[P_{2,2,2,1O1}]^+$	1.46		1.42	0.028	51.13	1.00
$[P_{2,2,2,2O1}]^+$	1.44		1.39	0.036	51.91	0.95

[a]Densities calculated or measured at 293 K.

4. RESULTS AND DISCUSSION

4.1. Liquid Density. Force field can be validated by several properties, including density,[11,13,15−17,20,21,24,26,29−31,33−36] diffusion constant,[12,13] neutron diffraction,[12,13] spectroscopic data,[14,25] crystal structure,[15,16,20,23,31,35] isothermal compressibility,[21] heat capacity,[11] melting point,[30] heat of vaporization,[33,34,36] etc. The density is most frequently used and it can be directly obtained from isothermal–isobaric MD simulations. Among all the density validations, most of the calculation error is below 3%;[13,15,20,26,30,31,34,35] however, in order to keep the consistency of the parameters, some of the calculation errors exceed 5%.[15,30,35] Based on the box sizes and the atom numbers, the atomic densities could be obtained. In order to compare conveniently, the relative atomic densities (d) were computed and are shown in Table 1. The predicted and experimental densities[6,49] are also listed in the table. It is seen that the simulated result are in good agreement with those measured experimentally except $[P_{1,1,1,6}][Tf_2N]$. It may be caused by the different parametrization of the carbons directly attached to the phosphorus atom. There are many instances where the methylated or ethylated members of a homologous series of compounds with a common alkyl side chain exhibit an outlier character.

The error for all the simulation results may be caused by several reasons. First, the LJ potential is not realistic enough to describe the interactions within these systems accurately. As a result, the agreement of simulated densities with the reference could be improved by fine-tuning the parameters for Lennard-Jones parameters. However, as Lopes suggested, keeping the

dx.doi.org/10.1021/jp210696r | J. Phys. Chem. B 2012, 116, 4934–4942

Table 2. Electrostatic, van der Waals (VDW), and Intermolecular Energy

	$[P_{1,1,1,6}]^+$	$[P_{2,2,2,5}]^+$	$[P_{2,2,2,8}]^+$	$[P_{2,2,2,12}]^+$	$[P_{4,4,4,14}]^+$	$[P_{8,8,8,8}]^+$	$[P_{2,2,2,1O1}]^+$	$[P_{2,2,2,2O1}]^+$
E_{ele} (kJ/mol)	−396.33	−368.25	−365.43	−362.30	−339.62	−331.44	−371.31	−375.05
E_{VDW} (kJ/mol)	−127.75	−135.80	−151.32	−171.04	−208.51	−234.21	−125.51	−131.12
E_{inter} (kJ/mol)	−524.08	−504.06	−516.75	−533.34	−548.14	−565.64	−496.83	−506.17
$E_{ion\ pair}$ (kJ/mol)	−291.23	−286.93	−276.03	−269.76	−282.80	−273.07	−289.01	−311.45
ΔU^{vap} (kJ/mol)	232.85	217.13	240.72	263.58	265.34	292.57	207.82	194.72
ΔH^{vap} (kJ/mol)	235.32	219.60	243.19	266.06	267.82	295.05	210.30	197.20

transferability of parameters between families of ionic liquids, we should only reparametrize geometrical parameters, torsion profiles, electron densities, and point charge distributions and leave the empirical nonbonded parameters unchanged.[35] Another point, the charges derived from gas-phase calculations do not necessarily represent charges in the liquid phase, particularly when the liquid is composed of associative ions prone to polarizability and charge transfer. Sometimes, the trace amounts of impurities, take water for example, which is difficult to remove completely could change the experimental density dramatically.

4.2. Liquid Energy. Looking into the electrostatic and van der Waals (VDW) contributions to the intermolecular interaction energy U_{inter} in Table 2, it is evident that the electrostatic interactions are significantly higher than the VDW interactions. As expected, the larger cation produces larger van der Waals interaction. However, the electrostatic interaction shows the opposite trend. In order to investigate the effect of alkyl chain length on the VDW and electrostatic interaction, we tried to associate the number of the alkyl chain length with the energy; however, no good result could be obtained. Then we summed up all the carbon atom numbers of the alkyl chain in each IL, and two lines are shown in Figure 3. Again,

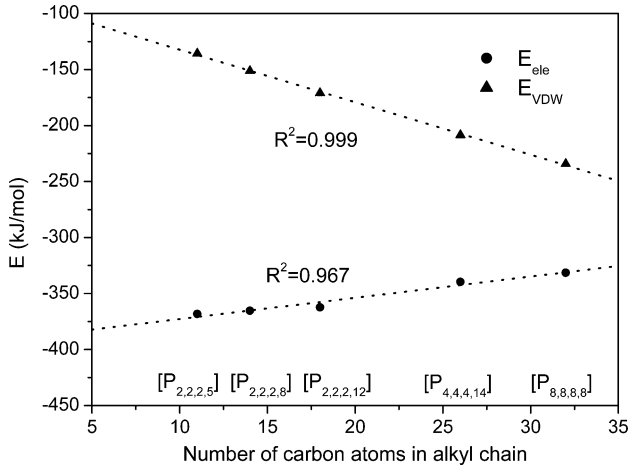

Figure 3. Association of the cation atom numbers of the alkyl chain with the VDW and Coulomb interactions.

$[P_{1,1,1,6}][Tf_2N]$ exhibits an outlier character and is not shown in the figure. Also from Table 2, it can be seen that changing the cation from $[P_{1,1,1,6}]^+$ to $[P_{8,8,8,8}]^+$ comes along with E_{inter} first decreasing and then increasing because of the competition between electrostatic and VDW contributions. Among all the six tetraalkylphosphonium-based ionic liquids, the interaction energy value for $[P_{2,2,2,5}]Tf_2N$ is the highest, and it is evident that the interaction between ions in $[P_{2,2,2,5}]Tf_2N$ is relatively lower than in the other five kinds of ILs. For the two kinds of alkoxyphosphonium ILs, the interactions are lower than most of these alkylphosphonium ILs.

ILs can be used in many chemical engineering processes. However, one of the bottlenecks is the high viscosity of ILs[14,23,48] In order to explore how the ionic interactions affect the dynamic properties, we plotted experimental viscosities under 298 K[6,49] and E_{inter} for $[P_{1,1,1,6}][Tf_2N]$, $[P_{2,2,2,5}][Tf_2N]$, $[P_{2,2,2,8}][Tf_2N]$, and $[P_{2,2,2,12}][Tf_2N]$ in Figure 4. It is obvious

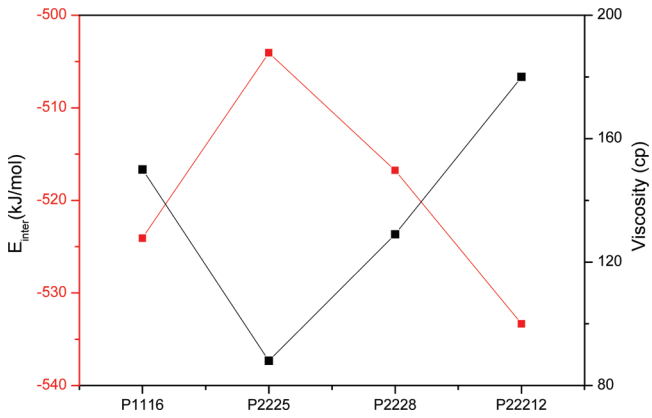

Figure 4. Experimental viscosities and E_{inter} for $[P_{1,1,1,6}][Tf_2N]$, $[P_{2,2,2,5}][Tf_2N]$, $[P_{2,2,2,8}][Tf_2N]$, and $[P_{2,2,2,12}][Tf_2N]$ under 298 K.

that the viscosity and interaction energy values show the opposite trend. The relatively high viscosities of ILs may due to the strong interactions between the ions. Considering the lower ionic interactions in $[P_{2,2,2,1O1}][Tf_2N]$ and $[P_{2,2,2,2O1}][Tf_2N]$, it is not surprising that both the two kinds of ILs exhibit low viscosities.[6]

The interaction energies between ionic pairs for these ILs were calculated by QM at the B3LYP/6-31+G(d) level, and the results are listed in Table 2. Based on the $E_{ion\ pair}$ and E_{int}, we could obtain the cohesive energy and vaporization enthalpy, which are defined as

$$\Delta U^{vap} = U^{ion\ pair} - U^{int} \quad (2)$$

$$\Delta H^{vap} = \Delta U^{vap} + RT \quad (3)$$

The results are listed in Table 2. It is found that, for the tetraalkylphosphonium-based ILs, ΔH^{vap} becomes larger with increasing length of alkyl chain except $[P_{1,1,1,6}][Tf_2N]$, and the most obvious examples are $[P_{2,2,2,5}][Tf_2N]$, $[P_{2,2,2,8}][Tf_2N]$, and $[P_{2,2,2,12}][Tf_2N]$.

4.3. Microstructures. *4.3.1. Radial Distribution Functions and Relative Density Distribution.* RDF is widely used to obtain insight into the organization of the liquid.[36,48,50] In this work, the site−site RDFs were computed. Figure 5, a and c, shows the RDFs for the central P atom in the cation and the central N atom in the anion, which could stand for the general interaction between cation and anion. All the eight kinds of

dx.doi.org/10.1021/jp210696r | J. Phys. Chem. B 2012, 116, 4934−4942

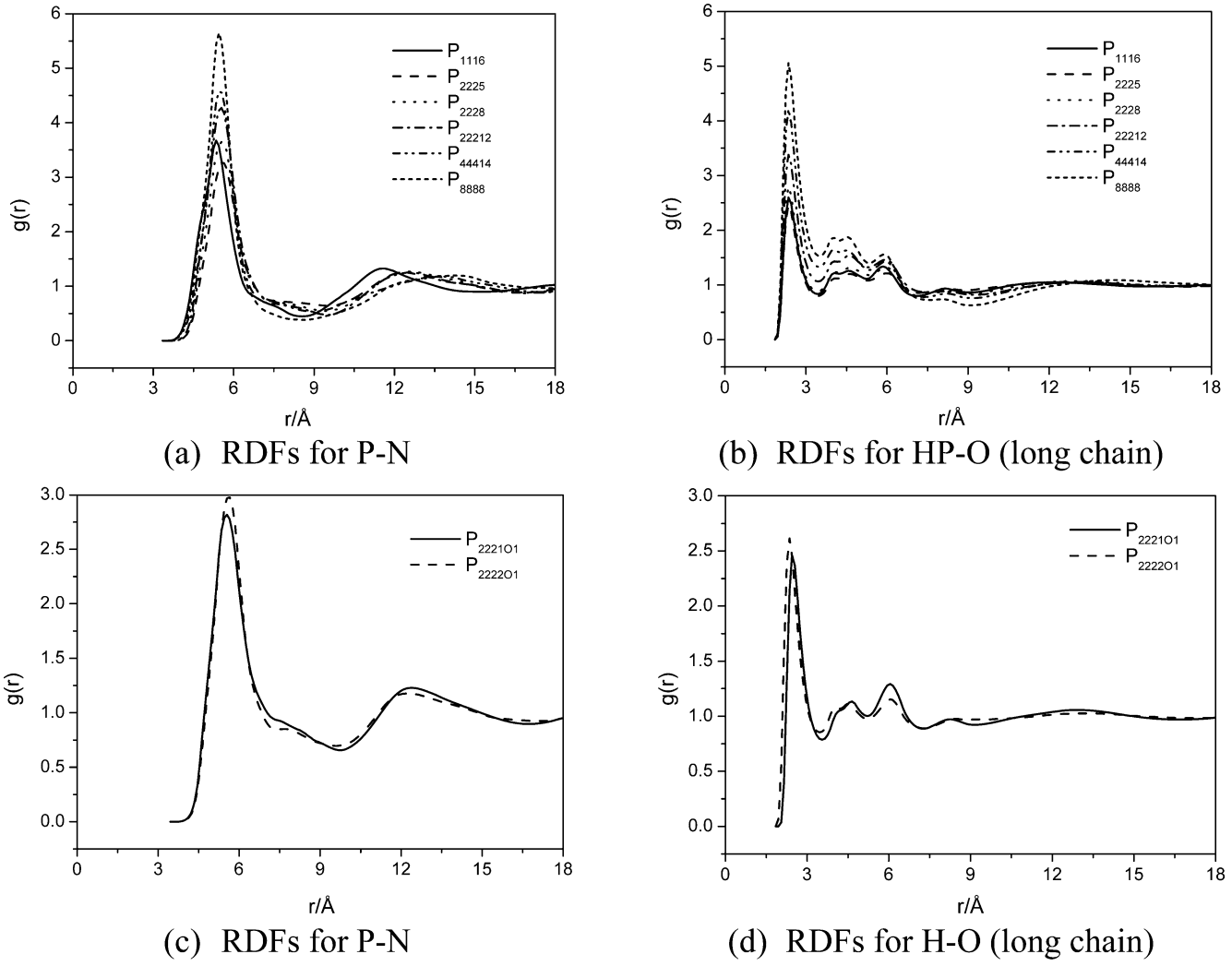

Figure 5. Radial distribution functions between P atom and N atom, and HP atom and O atom.

Table 3. Coordination Numbers for RDFs of P−N and HP−O in Phosphonium-Based ILs

type	$[P_{1,1,1,6}][Tf_2N]$	$[P_{2,2,2,5}][Tf_2N]$	$[P_{2,2,2,8}][Tf_2N]$	$[P_{2,2,2,12}][Tf_2N]$
P−N	5.26	6.09	5.26	4.83
HP−O[a]	0.38	0.32	0.31	0.32
HP−O[b]	0.36	0.37	0.37	0.36
type	$[P_{4,4,4,14}][Tf_2N]$	$[P_{8,8,8,8}][Tf_2N]$	$[P_{2,2,2,1O1}][Tf_2N]$	$[P_{2,2,2,2O1}][Tf_2N]$
P−N	3.37	2.72	7.47	6.82
HP−O[a]	0.31	0.34	0.39	0.37
HP−O[b]	0.31		0.37	0.35

[a]Long alkyl chain. [b]Short alkyl chain.

liquids exhibit a first cation−anion peak at approximately 5.5 Å and the long-range spatial correlations that extend to about 2 nm. The RDFs for H atoms in CH_2 connected with the central P and O atoms in anions are shown in Figure 5, b and d. All the eight RDFs exhibit a first peak at approximately 2.35 Å. From the above figures, it is obvious that the first peak height becomes more intense with increasing length of alkyl chain. It is in contrast with the traditional view that the interaction between ions becomes more difficult for ILs with longer alkyl chain due to the additional conformational flexibility and the steric hindrance.

The organization of the bulk liquid can also be analyzed by examining the coordination number, which is the average number of specific sites or atoms within a sphere of radius r about some other central sites or atoms. The coordination numbers can be calculated by integral of RDFs from zero to the first minimum.[17] The RDFs in Figure 5a,c were integrated and results are listed in Table 3. It is indicated from the P−N coordination number that each cation is surrounded by several anions. The shorter of the alkyl chain length, the more the anions will be. It is evident that interaction for ions becomes more difficult with increasing length of alkyl chain, which is in contrast with the conclusion of RDFs.

Considering the atomic density changes for different systems, the relative density distributions were used to depict the microstructures in these ILs. They are calculated by the

dx.doi.org/10.1021/jp210696r | J. Phys. Chem. B 2012, 116, 4934−4942

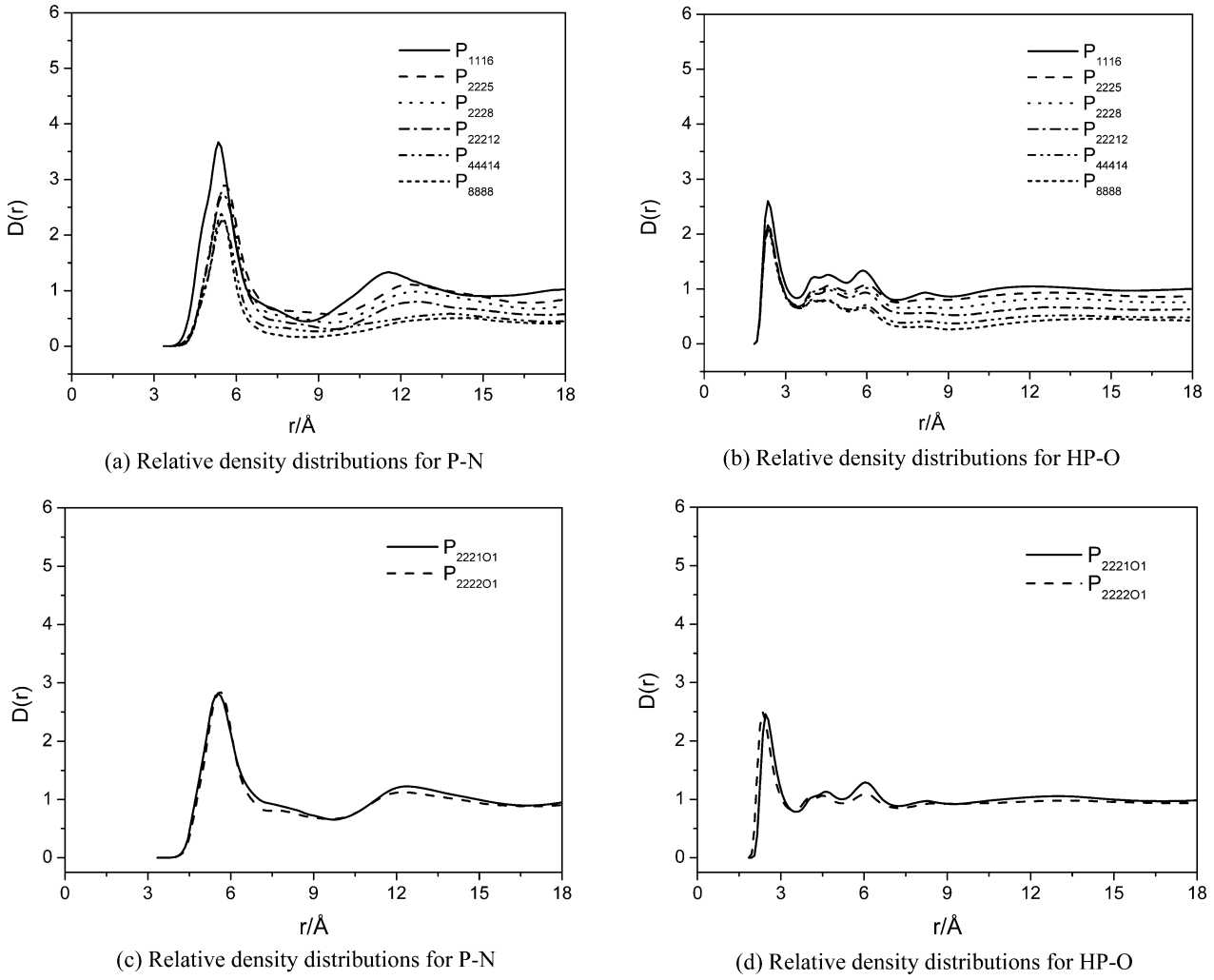

Figure 6. Relative density distributions for N atom around P atom and O atom around HP.

Table 4. Number of Hydrogen Bonds in Phosphonium-Based ILs

type	$[P_{1,1,1,6}]^+$	$[P_{2,2,2,5}]^+$	$[P_{2,2,2,8}]^+$	$[P_{2,2,2,12}]^+$	$[P_{4,4,4,14}]^+$	$[P_{8,8,8,8}]^+$	$[P_{2,2,2,1O1}]^+$	$[P_{2,2,2,2O1}]^+$
HP in short alkyl chain	0.30	0.24	0.25	0.24	0.20	0.20	0.24	0.23
HP in long alkyl chain	0.20	0.23	0.22	0.22	0.21		0.18	0.24
hydrogen bond in each cation with anion	1.11	0.96	0.97	0.94	0.82	0.80	0.90	0.92

following formula, where d stands for the relative atomic density, and are listed in Table 1.

$$\rho(r) = g(r)\cdot d \tag{4}$$

The relative density distributions for N atom around the central P atom and O atom around HP are presented in Figure 6. It is observed that the first peak height becomes less intense with increasing length of alkyl chain, which means the interaction between cation and anion becomes more difficult. It is consistent with the coordination number and the traditional view. For $[P_{2,2,2,1O1}][Tf_2N]$ and $[P_{2,2,2,2O1}][Tf_2N]$, the relative density distributions are almost the same.

4.3.2. Hydrogen Bond. It is known that the electrostatic interaction between ions is the most remarkable interaction in ILs. Besides the electrostatic interaction, hydrogen bond also plays an important role in the properties of ILs. For imidazolium-based ILs' hydrogen bonds, even the three-dimensional network has been found.[51] However, the hydrogen bond in phosphonium-based ILs has not been studied systemically. In this work, we calculated the number of hydrogen bonds for HP—O with the criteria as follows: H···O distance is less than 2.5 Å and C—H···O angle is larger than 150°. The calculated number of hydrogen bonds is listed in Table 4. Comparing the number of hydrogen bonds for each cation, we find that the order is $[P_{1,1,1,6}]^+ > [P_{2,2,2,5}]^+ > [P_{2,2,2,8}]^+ > [P_{2,2,2,12}]^+ > [P_{4,4,4,14}]^+ > [P_{8,8,8,8}]^+$. It is evident that hydrogen bonds form easily in the ILs with short alkyl chain. The hydrogen bond numbers for $[P_{2,2,2,1O1}][Tf_2N]$ and $[P_{2,2,2,2O1}][Tf_2N]$ are similar to each other. In order to show this more clearly, the hydrogen bond number combined with the anionic number interacting with cation through HP and O atoms for the six alkylphosphonium ILs are presented in Figure 7. The anionic number No. could be obtained by

$$\text{No.} = (n_L CN_L + n_S CN_S)/4 \tag{5}$$

dx.doi.org/10.1021/jp210696r | J. Phys. Chem. B 2012, 116, 4934–4942

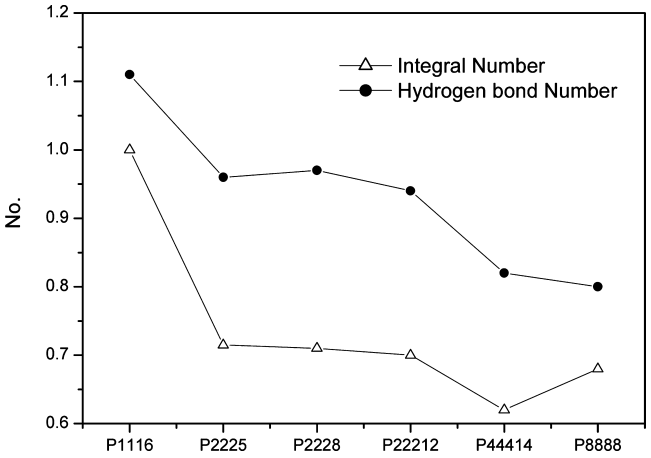

Figure 7. Hydrogen bond number and cationic number interaction with anion through O and HP atoms.

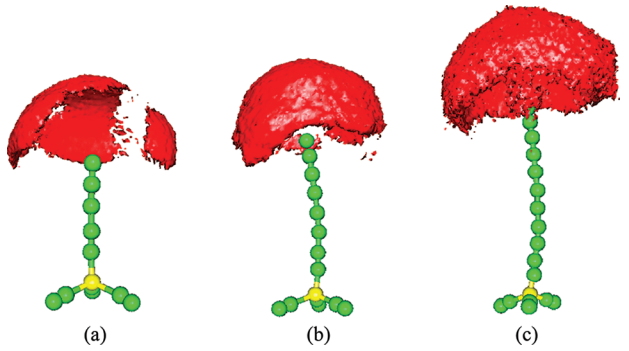

Figure 8. Spatial distribution functions (SDFs) for the end of CH_3 around cation: (a) $[P_{2,2,2,5}][Tf_2N]$, (b) $[P_{2,2,2,8}][Tf_2N]$, and (c) $[P_{2,2,2,12}][Tf_2N]$.

where n_L and n_S stand for the number of HP for each cation in the long and short alkyl chain, respectively. CN stands for the coordination number for O around HP. As there are four O atoms in each anion, it should be divided by 4. It is obvious from Figure 7 that the two lines are consistent with each other. The error may become less by using more strict criteria of hydrogen bond. Comparing the hydrogen bond number with coordination number for N atom around P atom, we can seen that, although several anions are found in the first solvation shell of cation, on average no more than one hydrogen bond forms for each IL pair. Less hydrogen bonds can be found with increasing length of alkyl chain. For $[P_{8,8,8,8}]Tf_2N$, no hydrogen bond is found for 20% of the cations. It is reported by Lorenzo Gontrani[8] that strong P−Cl interaction exists in $[P_{6,6,6,14}]Cl$ as the small chloride anion can reside very closely to the P atom. However, it is difficult for $[Tf_2N]^-$, a much larger ion, to reside closely to the $[P_{x,x,x,x}]^+$ cations.

4.3.3. Effect of Carbon Chain Length. In order to investigate the effect of carbon chain length on the structure, the space distribution functions (SDFs) were computed, which could stand for the probability of finding an atom in the three-dimensional space around a center ion/molecule. Among all the six tetraalkylphosphonium-based ILs, $[P_{2,2,2,5}][Tf_2N]$, $[P_{2,2,2,8}][Tf_2N]$, and $[P_{2,2,2,12}][Tf_2N]$ are the most comparable ones. Considering the atomic density differences, which are shown in Table 1, all the contours should be multiplied by the relative atomic density. The SDFs for the end CH_3 in the alkyl chain around the cation are shown in Figure 8. For example, the SDF for $[P_{2,2,2,12}][Tf_2N]$ stands for the 12th alkyl CH_3 around the cation. In the figure, the red contour surfaces are drawn at 3 times of the average density. From the figure, it is found that the probability of finding the end CH_3 is higher for the longer carbon chain length. The distribution of alkyl chain around the cations may be evidence for existence of the nanostructures in these ILs. However, the central cations' structures indicate that, although nanoscale segregation exists, the alkyl chain in $[P_{2,2,2,5}][Tf_2N]$ assumes an almost fully stretched configuration, while the longer chains in $[P_{2,2,2,8}][Tf_2N]$ and $[P_{2,2,2,12}][Tf_2N]$ show a little bending with no coiling. This is also observed by the experimental and simulation results for $[P_{6,6,6,14}]Cl$.[8]

5. CONCLUSIONS

In this work, force field was proposed for two kinds of the alkoxyphosphonium ILs through the Amber systematic method. Molecular dynamics simulations were performed for the alkoxyphosphonium ILs and six kinds of tetraalkylphosphonium ILs. Density was used to validate the force field parameters, and good agreement was obtained. Based on the simulations, it is found that E_{inter} first decreases and then increases with changing the cation from $[P_{1,1,1,6}]^+$ to $[P_{8,8,8,8}]^+$, while the viscosity presents the opposite trend. We come to the conclusion that the relatively high viscosities of ILs may be due to the strong interaction, including the electrostic force and van der Waals force. It may be a good explanation that $[P_{2,2,2,1O1}][Tf_2N]$ and $[P_{2,2,2,2O1}][Tf_2N]$ exhibit low viscosities. RDFs were calculated to depict the microstructures and interactions between ions; however, it is obvious that the first peak height becomes more intense with increasing length of alkyl chain which may involve counterintuitive conclusions. Considering the density difference, relative density distribution was applied. We found that the first peak height becomes less intense with increasing length of alkyl chain. It indicates that the interaction between ions becomes more difficult, which is consistent with the coordination number based on integral of the RDFs and the traditional view. The number of hydrogen bonds for HP−O was calculated, and hydrogen bond forms easily in the ILs with short alkyl chain. Combined with the anionic number interaction with cation through HP and O atoms, it is evident that, although several anions are found in the first solvation shell of cation, no more than one hydrogen bond forms in these ILs on average. Based on the SDFs, it is indicated that, although nanoscale segregation exists, the alkyl chains in the three ILs may show a stretched configuration or a little bending with no coiling.

■ ASSOCIATED CONTENT

Ⓢ Supporting Information

All the parameters of the force fields for the cations can be found in Table S1. This material is available free of charge via the Internet at http://pubs.acs.org.

■ AUTHOR INFORMATION

Notes

The authors declare no competing financial interest.

■ ACKNOWLEDGMENTS

This work was supported by the National Basic Research Program of China (973 Program, 2009CB219902), General Program Youth of National Natural Science Foundation of

China (20903098, 21106146), and State Key Laboratory of Multiphase Complex Systems (MPCS-2011-D-05).

REFERENCES

(1) Duffy, N. W.; Bond, A. M. *Electrochem. Commun.* **2006**, *8* (5), 892−898.
(2) Pringle, J. M.; MacFarlane, D. R.; Forsyth, M. *Synth. Met.* **2005**, *155* (3), 684−689.
(3) Frackwiak, E.; Lota, G.; Pernak, J. *Appl. Phys. Lett.* **2005**, *86* (16), 164101−164103.
(4) Ramirez, R. E.; Sanchez, E. M. *Sol. Energy Mater. Sol. Cells* **2006**, *90* (15), 2384−2390.
(5) Ramirez, R. E.; Torres-Gonzalez, L. C.; Sanchez, E. M. *J. Electrochem. Soc.* **2007**, *154* (2), B229−B233.
(6) Tsunashima, K.; Sugiya, M. *Electrochem. Commun.* **2007**, *9* (9), 2353−2358.
(7) Fraser, K. J.; Izgorodina, E. I.; Forsyth, M.; Scott, J. L.; MacFarlane, D. R. *Chem. Commun.* **2007**, *39*, 3817−3819.
(8) Gontrani, L.; Russina, O.; Celso, F. L.; Caminiti, R.; Annat, G.; Triolo, A. *J. Phys. Chem. B* **2009**, *113*, 9235−9240.
(9) Liu, X.; Zhou, G.; Zhang, S.; Yu, G. *Mol. Simul.* **2010**, *36* (1), 79−86.
(10) Kowsari, M. H.; Alavi, S.; Najafi, B.; Gholizadeh, K.; Dehghanpisheh, E.; Ranjbar, F. *Phys. Chem. Chem. Phys.* **2011**, *13* (19), 8826−8837.
(11) Zhou, G.; Liu, X.; Zhang, S.; Yu, G.; He, H. *J. Phys. Chem. B* **2007**, *111*, 7078−7084.
(12) de Andrade, J.; Boles, E. S.; Stassen, H. *J. Phys. Chem. B* **2002**, *106*, 3546−3548.
(13) de Andrade, J.; Boles, E. S.; Stassen, H. *J. Phys. Chem. B* **2002**, *106*, 13344−13351.
(14) Morrow, T. I.; Maginn, E. J. *J. Phys. Chem. B* **2002**, *106*, 12807−12813.
(15) Lopes, J. N. C.; Deschamps, J.; Pádua, A. l. A. H. *J. Phys. Chem. B* **2004**, *108*, 2038−2047.
(16) Lopes, J. N. C.; Pádua, A. l. A. H. *J. Phys. Chem. B* **2004**, *108*, 16893−16898.
(17) Liu, Z.; Huang, S.; Wang, W. *J. Phys. Chem. B* **2004**, *108*, 12978−12989.
(18) Yan, T.; Burnham, C. J.; Pópolo, M. G. D.; Voth, G. A. *J. Phys. Chem. B* **2004**, *108*, 11877−11881.
(19) Liu, Z.; Wu, X.; Wang, W. *Phys. Chem. Chem. Phys.* **2006**, *8* (9), 1096−1104.
(20) Lopes, J. N. C.; Pádua, A. l. A. H. *J. Phys. Chem. B* **2006**, *110*, 19586−19592.
(21) Micaelo, N. M.; Baptista, A. n. M.; Soares, C. u. M. *J. Phys. Chem. B* **2006**, *110*, 14444−14451.
(22) Youngs, T. G. A.; Pópolo, M. G. D.; Kohanoff, J. *J. Phys. Chem. B* **2006**, *110*, 5697−5707.
(23) Cadena, C.; Maginn, E. J. *J. Phys. Chem. B* **2006**, *110* (36), 18026−18039.
(24) Liu, X.; Zhang, S.; Zhou, G.; Wu, G.; Yuan, X.; Yao, X. *J. Phys. Chem. B* **2006**, *110*, 12062−12071.
(25) Lopes, J. N. A. C.; Pádua, A. l. A. H. *J. Phys. Chem. B* **2006**, *110*, 7485−7489.
(26) Wang, Y.; Pan, H.; Li, H.; Wang, C. *J. Phys. Chem. B* **2007**, *111*, 10461−10467.
(27) Bagno, A.; D'Amico, F.; Saielli, G. *J. Mol. Liq.* **2007**, *131*−*132* (SI), 17−23.
(28) Acevedo, O.; Jorgensen, W. L.; Evanseck, J. D. *J. Chem. Theory Comput.* **2007**, *3* (1), 132−138.
(29) Liu, X.; Zhou, G.; Zhang, S.; Wu, G.; Yu, G. *J. Phys. Chem. B* **2007**, *111*, 5658−5668.
(30) Klähn, M.; Seduraman, A.; Wu, P. *J. Phys. Chem. B* **2008**, *112*, 10989−11004.
(31) Lopes, J. N. C.; Pádua, A. l. A. H.; Shimizu, K. *J. Phys. Chem. B* **2008**, *112*, 5039−5046.
(32) Zhang, X.; Huo, F.; Liu, Z.; Wang, W.; Shi, W.; Maginn, E. J. *J. Phys. Chem. B* **2009**, *113*, 7591−7598.
(33) Sambasivarao, S. V.; Acevedo, O. *J. Chem. Theory Comput.* **2009**, *5* (4), 1038−1050.
(34) Borodin, O. *J. Phys. Chem. B* **2009**, *113*, 11463−11478.
(35) Shimizu, K.; Almantariotis, D.; Gomes, M. F. C.; Pádua, A. l. A. H.; Lopes, J. N. C. *J. Phys. Chem. B* **2010**, *114*, 3592−3600.
(36) Liu, Z.; Chen, T.; Bell, A.; Smit, B. *J. Phys. Chem. B* **2010**, *114*, 4572−4582.
(37) Liu, X.; Zhou, G.; Zhang, S. *Fluid Phase Equilib.* **2008**, *272* (1−2), 1−7.
(38) MacKerell, A. D.; Bashford, D.; Bellott, M.; Dunbrack, R. L.; Evanseck, J. D.; Field, M. J.; Fischer, S.; Gao, J.; Guo, H.; Ha, S.; et al. *J. Phys. Chem. B* **1998**, *102*, 3586−3616.
(39) Xie, H.; Zhang, S.; Duan, H. *Tetrahedron Lett.* **2004**, *45* (9), 2013−2015.
(40) Cornell, W. D.; Cieplak, P.; Bayly, C. I.; Gould, I. R.; Merz, K. M.; Ferguson, D. M.; Spellmeyer, D. C.; Fox, T.; Caldwell, J. W.; Kollman, P. A. *J. Am. Chem. Soc.* **1995**, *117*, 5179−5197.
(41) Fox, T.; Kollman, P. A. *J. Phys. Chem. B* **1998**, *102*, 8070−8079.
(42) Cornell, W. D.; Cieplak, P.; Bayly, C. I.; Kollmann, P. A. *J. Am. Chem. Soc.* **1993**, *115*, 9620−9631.
(43) Cieplak, P.; Cornell, W. D.; Bayly, C.; Kollman, P. A. *J. Comput. Chem.* **1995**, *16* (11), 1357−1377.
(44) Wang, J. M.; Cieplak, P.; Kollman, P. A. *J. Comput. Chem.* **2000**, *21* (1049), 1049−1074.
(45) Pappu, R. V.; Hart, R. K.; Ponder, J. W. *J. Phys. Chem. B* **1998**, *102*, 9725−9742.
(46) Lyubartsev, A. P.; Laaksonen, A. *Comput. Phys. Commun.* **2000**, *128* (3), 565−589.
(47) Martyna, G. J.; Tuckerman, M. E.; Tobias, D. J.; Klein, M. L. *Mol. Phys.* **1996**, *87* (5), 1117−1157.
(48) Cadena, C.; Zhao, Q.; Snurr, R. Q.; Maginn, E. J. *J. Phys. Chem. B* **2006**, *110*, 2821−2832.
(49) Sesto, R. E. D.; Corley, C.; Robertson, A.; Wilkes, J. S. *J. Organomet. Chem.* **2005**, *690* (10), 2536−2542.
(50) Rey-Castro, C.; Vega, L. F. *J. Phys. Chem. B* **2006**, *110*, 14426−14435.
(51) Dong, K.; Zhang, S.; Wang, D.; Yao, X. *J. Phys. Chem. A* **2006**, *110*, 9775−9782.